



Research paper



Exploring *Asphodelus microcarpus* as a source of xanthine oxidase inhibitors: Insights from in silico and in vitro studies

Amalia Di Petrillo^{a,*}, Chiara Siguri^{b,1}, Giovanna L. Delogu^c, Antonella Fais^c, Benedetta Era^c, Sonia Floris^c, Francesca Pintus^c, Amit Kumar^d, Massimo Claudio Fantini^a, Stefania Olla^b

^a Department of Medical Sciences and Public Health, University of Cagliari, 09042, Monserrato, Italy

^b Institute for Genetic and Biomedical Research (IRGB), The National Research Council (CNR), 09042, Monserrato, Italy

^c Department of Life and Environmental Sciences, University of Cagliari, 09042, Monserrato, Italy

^d Department of Electrical and Electronic Engineering, University of Cagliari, Via Marengo 2, 09123, Cagliari, Italy

ARTICLE INFO

Keywords:

Xanthine oxidase
Molecular docking
Luteolin derivatives
Molecular dynamics

ABSTRACT

Xanthine oxidase (XO) plays a critical role in purine catabolism, catalyzing the conversion of hypoxanthine to xanthine and xanthine to uric acid, contributing to superoxide anion production. This process is implicated in various human diseases, particularly gout. Traditional XO inhibitors, such as allopurinol and febuxostat, while effective, may present side effects.

Our study focuses on *Asphodelus microcarpus*, a plant renowned for traditional anti-inflammatory uses. Recent investigations into its phenolic-rich flowers, notably abundant in luteolin derivatives, reveal its potential as a natural source of XO inhibitors. In the present research, XO inhibition by an ethanolic flowers extract from *A. microcarpus* is reported. *In silico* docking studies have highlighted luteolin derivatives as potential XO inhibitors, and molecular dynamics support that luteolin 7-O-glucoside has the highest binding stability compared to other compounds and controls. *In vitro* studies confirm that luteolin 7-O-glucoside inhibits XO more effectively than the standard inhibitor allopurinol, with an IC₅₀ value of 4.8 µg/mL compared to 11.5 µg/mL, respectively. These findings underscore the potential therapeutic significance of *A. microcarpus* in managing conditions related to XO activity. The research contributes valuable insights into the health-promoting properties of *A. microcarpus* and its potential application in natural medicine, presenting a promising avenue for further exploration in disease management.

1. Introduction

Xanthine oxidase (XO; EC 1.17.3.2) is a molybdenum-containing enzyme that plays a critical role in purine catabolism; it catalyzes the oxidation of hypoxanthine to xanthine and xanthine to uric acid (UA) with the production of superoxide anion [1](Fig. 1). At the heart of XO's catalytic mechanism lies the dioxothiomolybdenum (VI) ion, serving as the essential active site [2]. This molybdenum cofactor is intricately involved in the enzyme's oxidation-reduction reactions, enabling the oxygen transfer from water to the substrate. XO is necessary for normal human purine metabolism and is implicated in multiple human diseases due to its ability to generate UA and reactive oxygen species (ROS) [3]. Several 3D structures of XO are available in the Protein Data Bank (<http://www.rcsb.org/>), facilitating the study of the enzyme's interaction

mechanism by examining its binding site (Fig. S1).

The accumulation of UA has been shown to initiate the inflammatory process through NLRP3 inflammasome and the production of free radicals, which contribute to inflammation-related tissue damage [4]. Deposition of UA crystals or its monosodium salt in human joints with accompanying joint inflammation is the primary cause of gout [5]. Furthermore, the formation of ROS contributes to oxidative stress and cellular damage.

Two inhibitors of XO, allopurinol and febuxostat, that act as competitive and non-competitive inhibitors respectively, have been approved by the Food and Drug Administration to treat gout [6]. Although the therapeutic agent allopurinol has been identified as an effective treatment for gout, side effects of these traditional agents, such as bone marrow depression, allergic reactions, renal and gastrointestinal

* Corresponding author.

E-mail address: amalia.dip@unica.it (A. Di Petrillo).

¹ These authors contributed equally to this work.

toxicities, should not be overlooked [7].

Recent studies have turned the spotlight on flavonoids, a class of plant-derived phenolic compounds prevalent in a variety of fruits and vegetables [8]. These compounds are renowned for their antioxidant, anti-inflammatory, and antiproliferative actions [9]. Luteolin, a specific flavonoid, has demonstrated significant anti-hyperuricemic and anti-inflammatory effects, positioning it as a potential natural XO inhibitor [10].

Our focus extends to *Asphodelus microcarpus*, a Liliaceae family plant long valued in traditional medicine for its anti-inflammatory properties [11]. Recent scientific investigations have begun to unravel the basis of its ethnopharmacological applications, revealing its rich phenolic content and antioxidant capabilities, particularly in its flowers, which contain significant amounts of luteolin and its derivatives [12,13]. Luteolin (3',4',5,7-tetrahydroxyflavone) has a significant XO inhibitory activity compared with allopurinol [14]. In light of these findings, our objective is to explore the potential of *A. microcarpus* extract as a possible XO inhibitor and a valuable source of natural compounds capable of efficiently inhibiting XO.

Through this exploration, we aim to unlock the therapeutic potential of *A. microcarpus* in the context of natural medicine, further contributing to our understanding of its health-promoting properties.

2. Materials and methods

2.1. Materials

All reagents for biological assays were purchased from Sigma-Aldrich, unless otherwise indicated, and used without further purification.

2.2. Plants materials

Asphodelus microcarpus subsp. *microcarpus* Salzm. et Viv. leaves, flowers and tubers (L, F and T respectively) were collected, and a voucher specimen (1405/16 Herbarium CAG) has been deposited in the Department of Life and Environmental Sciences. Plant materials were washed with deionized water, frozen at -80°C and then lyophilized in intact condition.

2.3. Preparation of the extracts

The lyophilized plant materials (10 g) were extracted in 100 mL of ethanol (EE), methanol (ME) and aqueous (AE) for 24 h at room temperature under continuous stirring. After filtration, EE and ME were concentrated under reduced pressure to evaporate the alcohol. The aqueous phase was first frozen at -80°C and then lyophilized. Dried powders (1 mg) were dissolved in 1 mL of dimethyl sulfoxide (DMSO) before use.

2.4. Determination of enzyme inhibitory properties

The inhibitory activity of the extracts and synthetic compound against XO was obtained by measuring the formation of UA at 295 nm

[15]. The reaction mixture contained 0.1 M phosphate buffer solution (pH 7.5, 879 μL), an aqueous solution of XO from bovine milk (0.5 U/mL, 50 μL), and a sample solution or DMSO (10 μL). Then, xanthine solution (0.82 mM, 61 μL) was added, and the XO activity was determined at 295 nm for 3 min at 25°C . Allopurinol was used as a standard inhibitor. The IC_{50} value (concentration giving 50 % inhibition of XO activity), was determined for the most active extract and synthetic compound by the interpolation of dose-response curves.

The inhibition mode of the enzyme was performed using the Lineweaver-Burk plot. Enzyme kinetics was determined in the absence and presence of various concentrations of FEE (Flower Ethanol Extract) (10, 20, and 50 $\mu\text{g}/\text{mL}$) or luteolin 7-*O*-glucoside (1, 2.5, and 5 $\mu\text{g}/\text{mL}$) with varying concentrations of xanthine as substrate (4–16 μM).

The equilibrium constants for binding with the free enzyme (K_I) and with the enzyme-substrate complex (K_{IS}) have been obtained either from the slope (K_m/V_{max}) or the $1/V_{\text{max}}$ values plotted versus the inhibitor concentration, respectively.

2.5. Cell viability

Caco-2 cells were cultured under standard conditions (5 % CO_2 , 95 % relative humidity, and 37°C) in Dulbecco's Modified Eagle's Medium plus 1 % penicillin/streptomycin (Euroclone, Milan, Italy) and 10 % fetal bovine serum (Gibco, Grand Island, NY, USA). Cell viability was measured by the 3-(4,5-dimethylthiazol-2-yl)-2,5-diphenyltetrazolium bromide (MTT) assay [16]. Briefly, the cells were seeded in 96-well plates (5000 cells/well) and exposed for 24 h to FEE solution (2 mg/mL in DMSO) properly diluted to reach the required extract concentrations (0.1, 1, 2.5, 5, 10, 25, 50, and 100 $\mu\text{g}/\text{mL}$). Thereafter, the MTT solution (0.5 mg/mL) was added. After 3 h, DMSO was added to dissolve the formazan crystals, and the absorbance was recorded at 590 nm.

2.6. Antioxidant activity in cells

The antioxidant activity of FEE was assessed by analyzing the intracellular ROS levels via the 2',7'-dichlorofluorescein diacetate (DCFH-DA) method as previously described [17]. Caco-2 cells were incubated with the extract diluted to achieve the required concentrations (0.1, 1, 2.5, 5, 10, 25, 50, and 100 $\mu\text{g}/\text{mL}$) for 24 h. Then, the cells were incubated with 10 μM DCFH-DA for 30 min at 37°C . After the incubation, 2 mM of H_2O_2 was added to each well, and the fluorescence intensity of ROS-oxidized 2',7'-dichlorofluorescein (DCF) was measured at 485/530 nm (excitation/emission wavelengths), recording data for 60 min.

2.7. In silico studies

2.7.1. Protein and ligands preparation

On Protein Data Bank [18] we selected all the structures that exhibited no mutations in the amino acid sequence and contained molybdenum within the active site, resulting in 8 X-rays structures. The PDB IDs of selected 3D-structures are 1FIQ [19], 3EUB [20], 3NRZ [21], 3NVV [22], 3NVW [23], 3NVY [24]. Only one monomer was retained,

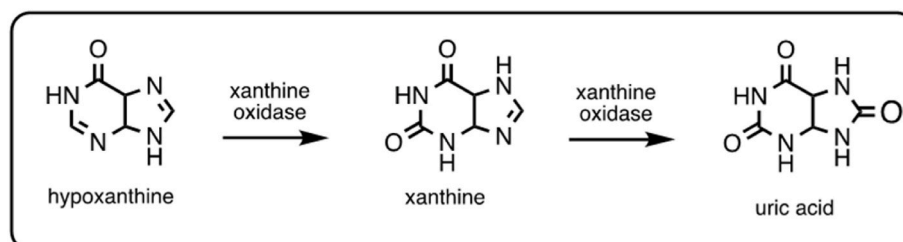


Fig. 1. Xanthine oxidase reaction converting hypoxanthine to xanthine and uric acid.

and with molybdenum ion was kept as it serves as a cofactor. The 8 structures were prepared using the Protein Preparation Wizard tool (Schrodinger Release 2022-3) [25], all hydrogen atoms were added, bond orders were adjusted, and formal charges were assigned. For only one X-ray (3UNA), the missing loops extending from Lys 165 to Ser 192, from Lys 529 to Gly 536, and from Val 1318 to Cys 1325 have been

added and they are not part of the active site. The appropriate ionization state was determined at pH 7.4 using the PROPKA tool [26], and the residues His 741 and His 875, located within 8 Å of the binding site, have been changed to HIE in all structures. The protein minimization by OPLS4 force field to fix all molecular overlaps and strains was then performed. The restrained minimization was terminated when the

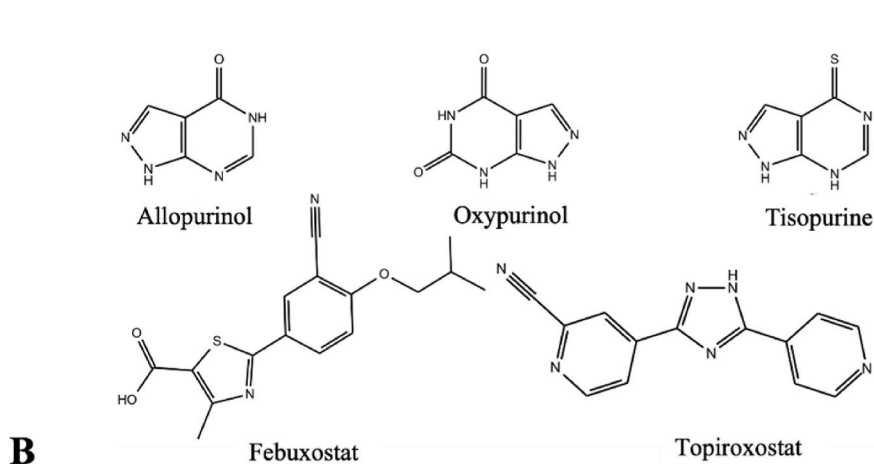
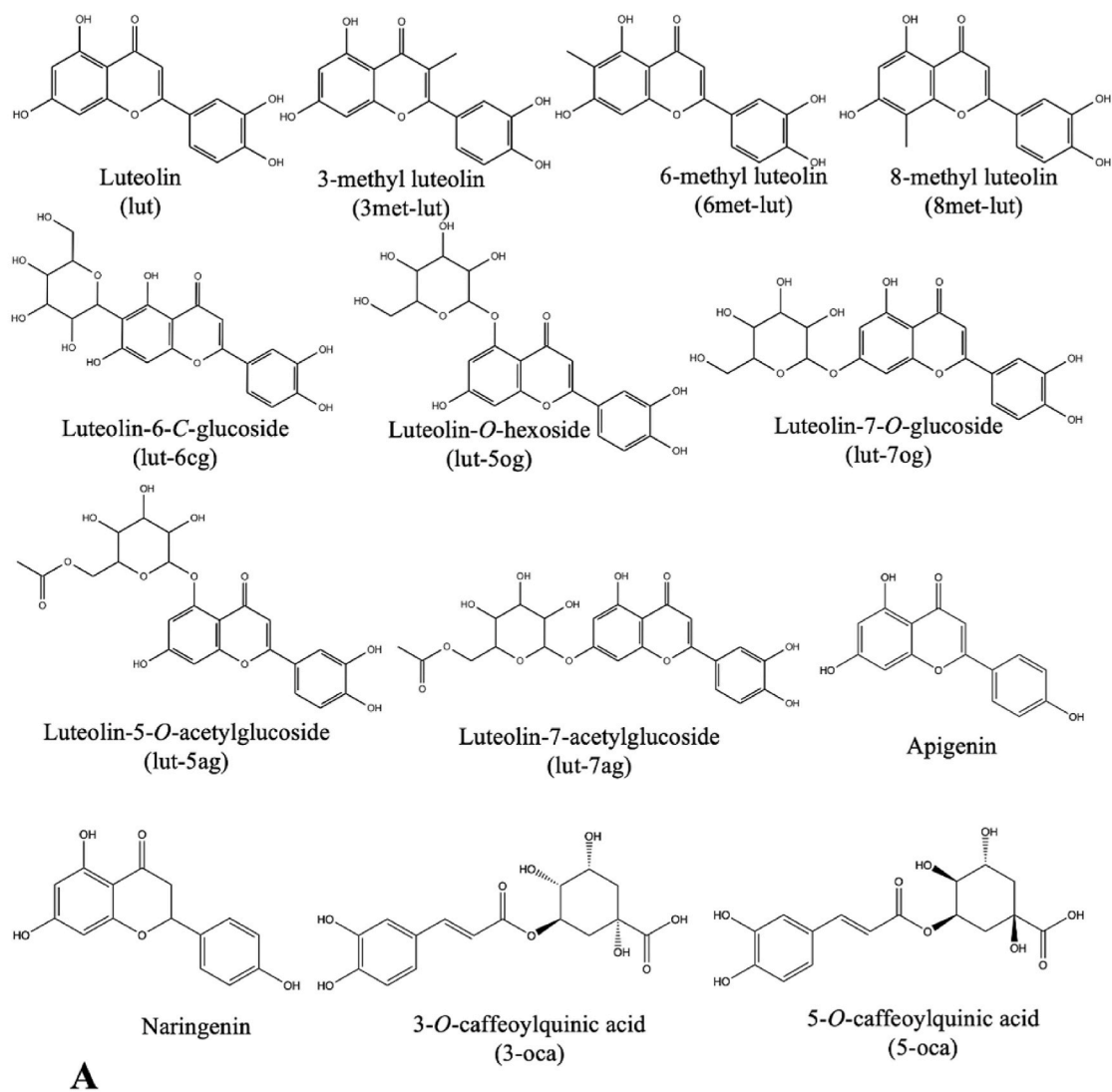


Fig. 2. Chemical structures of docked ligands. A: ligand set. B: known ligands of XO (control set).

average root mean square deviation (RMSD) of the non-hydrogen atoms was converged to 0.3 Å.

Compounds tentatively identified in prior analyses of FEE by Di Petrillo et al. [13] (Fig. 2A) and the control set consisting of allopurinol, febuxostat, oxypurinol, tisopurine, and topiroxostat, known XO inhibitors (Fig. 2B), were retrieved from PubChem or drawn with ChemDraw, and were then subjected to conformational analysis using the Quantomechanic Conformer and Tautomer Prediction tool from Jaguar (Schrödinger Release 2022–3) [27].

The best conformations were prepared with LigPrep (Schrödinger Release 2022–3) using the OPLS4 force field [28], generating the possible ionization states at pH 7.0 ± 2.0 , and retaining the specified chirality. The compounds with undetermined sugar positions were searched in literature and docked at the available position with the exception of luteolin-*O*-deoxysylhexoside where the possibilities were multiple and was therefore omitted. Compounds identified in analyses of FEE with respective docked compounds and acronyms used are reported in Fig. 2.

2.7.2. DFT calculations

Jaguar was also employed to perform the Density Functional Theory (DFT) calculations [29] using the B3LYP (Becke's three-parameter exchange potential and Lee-Yang-Parr correlation function) method [30] combined with the 6–311++G (d, p) basis set in water solvent. The following properties of the ligands were calculated: HOMO (Highest Occupied Molecular Orbital) and LUMO (Lowest Unoccupied Molecular Orbital) energies and their energy gap (ΔE).

2.7.3. Docking studies

2.7.3.1. Glide docking. The Receptor Grid Generator was employed, the centroid of the residues belonging to the binding site were selected as the center of the grid whose dimensions were $46 \times 46 \times 46$ Å. Glide-XP (Schrödinger Release 2022–3) [25,31] was chosen as one of the docking protocols and the OPLS_2005 [28] was used as the force field.

The results from the dockings were then submitted to MMGBSA (Molecular Mechanics with Generalized Born and Surface Area solvation) [32] calculations using Prime (Schrödinger Release 2022–3), choosing VSGB [33] as the solvation model and OPLS4 as the force field.

2.7.3.2. AutoDock. Gasteiger charges [34] were assigned and the grids were generated using AutoGrid [35] with established dimensions of $60 \times 60 \times 60$ Å, centered within the binding site.

For AutoDock [36], docking experiments were carried out using the Lamarckian genetic algorithm [37,38], a total of 250 runs were performed with a population size of 250 individuals, and maximum numbers of evaluation were set at 25,000,000. Other parameters were kept as defaults.

2.7.3.3. Ranking. The best pose of each compound in all x-rays for all docking procedures was selected. For each crystal, compounds with the best results were assigned a score of 1, the second-best a score of 2, and so on until the end, creating three separate tables (Glide-XP, MMGBSA and AutoDock). For each compound, the results obtained individually from the three procedures were summed to obtain the final ranking.

The lower the score, the better the compound.

2.7.4. Molecular dynamics

The three best compounds and febuxostat as control, underwent molecular dynamics (MD) studies based on the optimal poses obtained from docking programs on the 3NVV structure [24], where the best overall performances were observed for the three lead compounds.

MD studies were conducted using Desmond (Schrödinger Release 2022–3) [39], and the TIP3P solvent model [40] was utilized in conjunction with the OPLS4 force field [28]. To set up the system, each

complex was positioned in an orthorhombic water box with a 10.0 Å extension, and it underwent both minimization and neutralization via the introduction of Na^+ or Cl^- . The simulations extended for 250 ns, with trajectories recorded at intervals of 50 ps within the NPT ensemble. The temperature (300.0 K) and pressure (1.01325 bar) were consistently maintained using the Nosé-Hoover thermostat [41] and the Martyna-Tobias-Klein barostat [42] methods, respectively. Other parameters were kept at their default values. Analysis results were conducted using the Simulation Interaction Diagram tool integrated into Desmond, the obtained trajectories underwent post-MMGBSA analysis using the thermal_mmgbsa.py script. Additionally, trajectory frames were subjected to clustering based on ligand RMSD using the trj_cluster.py script [43]. Output files were generated for the five most populated clusters in each MD experiment. The interaction energies between the analyzed compounds and the active site residues, located within a radius of 4 Å and/or showing the most stable interactions, were calculated with the Schrödinger's analyze_simulation.py script.

2.7.5. In silico ADME predictions

QikProp (Schrödinger Release 2022–3) was utilized to predict the absorption, distribution, metabolism, and excretion (ADME) profile of luteolin and its derivatives. It utilizes an algorithm that establishes a correlation between experimentally determined properties and Monte Carlo statistical mechanics simulations. The properties that have been taken into consideration are the following: putative central nervous system activity (CNS), intestinal absorption, and possible oral bioavailability (apparent human colon carcinoma Caco-2 cell permeability in nm/sec, QPPCaco), CNS absorption (apparent Madin–Darby canine kidney cell permeability in nm/sec, QPPMDCK), number of likely metabolic reactions, qualitative and quantitative (on a 0–100 % scale) human oral absorption, number of violations of Lipinski's rule of five and Jorgensen's rule of three.

2.8. Statistical analysis

The results are reported as means \pm standard deviations (SD). Student's t-test was performed to substantiate differences between groups (i.e., the vesicle formulations). For cell viability and intracellular antioxidant activity data, a two-way analysis of variance (ANOVA) was performed using the type of extract (free or nano-formulated) and the different concentrations tested as variables, followed by Tukey's test, using GraphPad Prism software version 9 (San Diego, CA, USA). Differences were considered statistically significant for p values below 0.05.

3. Results

3.1. Xanthine oxidase inhibitory activity

The potential XO inhibitory activity of *A. microcarpus* extracts was first tested at a concentration of 0.2 mg/mL. Table 1 summarizes the percentage inhibition of XO by various extracts, along with the positive

Table 1

Percentage of XO inhibition by *A. microcarpus* extracts at 0.2 mg/mL concentration.

Part of the plant	Extracts	Inhibition (%)
Leaves	Aqueous	15.9 ± 1.2
	Ethanollic	40.2 ± 0.4
	Methanolic	23 ± 0.8
Flowers	Aqueous	6.5 ± 0.2
	Ethanollic	65.6 ± 4.5
	Methanolic	45.3 ± 4.6
Tubers	Aqueous	3.6 ± 0.8
	Ethanollic	8.4 ± 1.2
	Methanolic	9.2 ± 3.1

control, allopurinol. The FEE exhibited the most significant inhibition of XO (65.3 %) and the percentage inhibition value was significantly higher than that of other extracts ($p < 0.05$).

Considering that FEE exerted the best inhibitory activity, the IC_{50} value has been calculated and resulted to be $58.0 \pm 3.6 \mu\text{g/mL}$. This result is significant given that the extract is a complex mixture of compounds, where the concentration of active molecules is inherently lower than the total tested sample amount. Despite this, the extract's IC_{50} value surpasses that of the standard inhibitor allopurinol, which exhibits an IC_{50} of $11.5 \pm 0.8 \mu\text{g/mL}$, underscoring the potential of our extract as an effective XO inhibitor. Such findings highlight the therapeutic promise of naturally derived compounds in the management of conditions like hyperuricemia and gout.

In comparison, febuxostat demonstrated the most potent inhibitory activity with an IC_{50} of $0.05 \pm 0.002 \mu\text{g/mL}$, significantly outperforming both the extract and allopurinol. This aligns with literature that acknowledges febuxostat as a more effective XO inhibitor than allopurinol, though it is typically considered a second-line treatment option due to its adverse effects.

The kinetic behavior of XO at different concentrations of xanthine and FEE was also investigated. The Lineweaver-Burk plot gave a family of crossed straight lines with different slopes and y-intercepts which indicates that the compound is a mixed-type inhibitor of the enzyme (Fig. 3A). The inhibition constant (K_I) of $41 \mu\text{g/mL}$ was obtained from a plot of slope versus the inhibitor concentration (Fig. 3B) while the inhibition constant (K_{IS}) of $93.4 \mu\text{g/mL}$ was obtained from a plot of the vertical intercept ($1/V_{\text{max}}$) versus the inhibitor concentration (Fig. 3C). K_I and K_{IS} represent the equilibrium constants for binding of the inhibitor to the free enzyme or to the enzyme-substrate complex respectively.

3.2. Cell viability and anti-ROS activity

In order to investigate the potential antioxidant activity of FEE in a cellular model, the effect of the extract was first investigated on cell viability using Caco-2 as cell line.

A solution of FEE (2 mg/mL in DMSO) was properly diluted to reach the concentrations of 0.1, 1, 2.5, 5, 10, 25, 50 and 100 $\mu\text{g/mL}$. Caco-2 cells were treated with the FEE samples for 24 h, and the viability was investigated using the MTT test. The results indicated that none of the samples were cytotoxic in Caco-2 cells. A slight decrease, although not significant, in viability was observed in the cells exposed to the FEE solution, reaching the lower value (87.4 and 84.6 %) at the higher concentrations (50 and 100 $\mu\text{g/mL}$) (Fig. 4)

Since concentrations of FEE up to 100 $\mu\text{g/mL}$ do not affect the cell viability, we performed antioxidant cellular experiments using up to this concentration. ROS levels in cells were evaluated before and after H_2O_2 -induced oxidative stress and upon treatment with FEE. The experiment was performed by using the DCFHDA assay. Following this method, H_2O_2 -generated ROS in the cytoplasm oxidate DCFH to fluorescent DCF, whose levels were quantified spectrophotometrically. As shown in Fig. 4, the incubation of the Caco-2 cells with H_2O_2 significantly increased ROS levels (T vs NT cells). Treatment with FEE prevented ROS production in a dose-dependent manner (Fig. 5). The ROS concentration decreases while increasing the extract concentration and this result demonstrated the antioxidant effect of FEE in the cellular system.

3.3. In silico studies

3.3.1. Docking results

The eight XO X-ray structures used for docking are reported in Section 2.7.1 and for all structures, 18 compounds (Fig. 2) were docked using Glide-XP and AutoDock.

The XP-Gscores and MMGBSAs of the ligand docked are reported in Table S1 while AutoDock results are reported in Table S2. All ligand set studied showed better XP-Gscores than the control set except for febuxostat in Glide-XP docking. In order, the ligands with better ranking

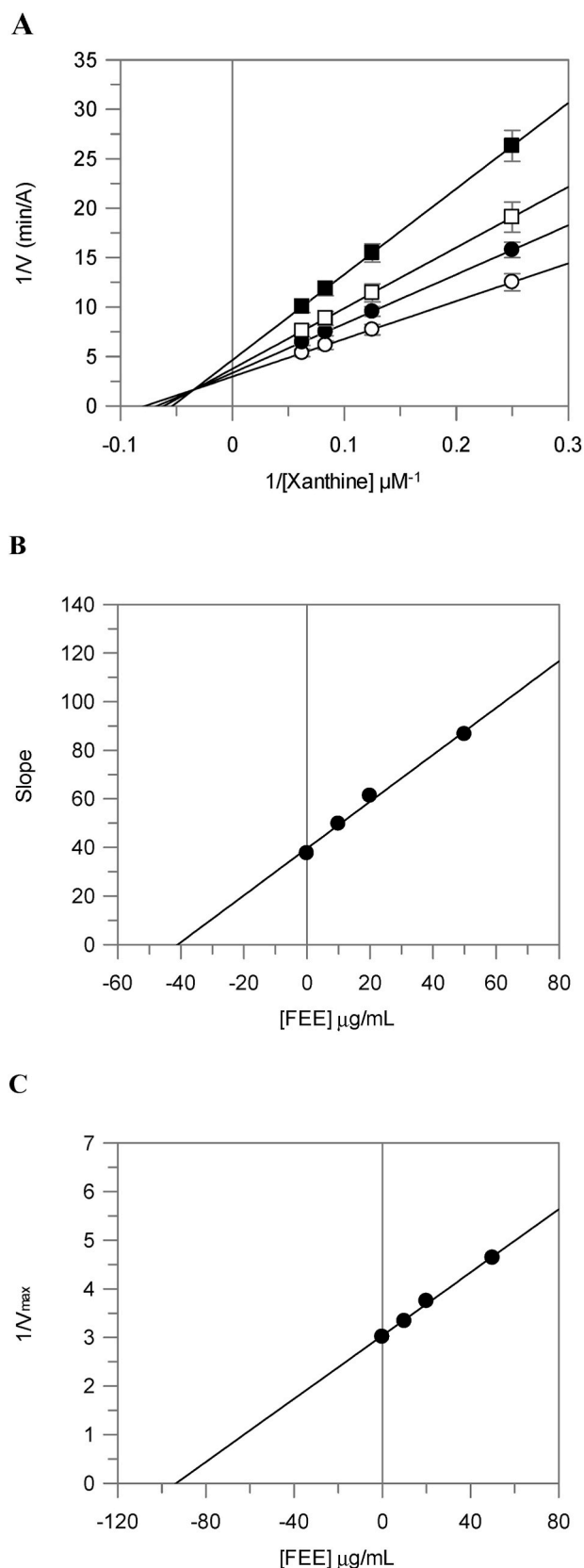


Fig. 3. Inhibition of XO activity by *A. microcarpus* flowers extract. A: Lineweaver-Burk plot for inhibition of FEE on XO activity using xanthine as substrate. Concentrations of extract were: 0 (●), 15 $\mu\text{g/mL}$ (○), 20 $\mu\text{g/mL}$ (■) and 50 $\mu\text{g/mL}$ (□). B: Replot of the slope values versus extract concentration. C: Replot of the $1/V_{\text{max}}$ values versus extract concentration.

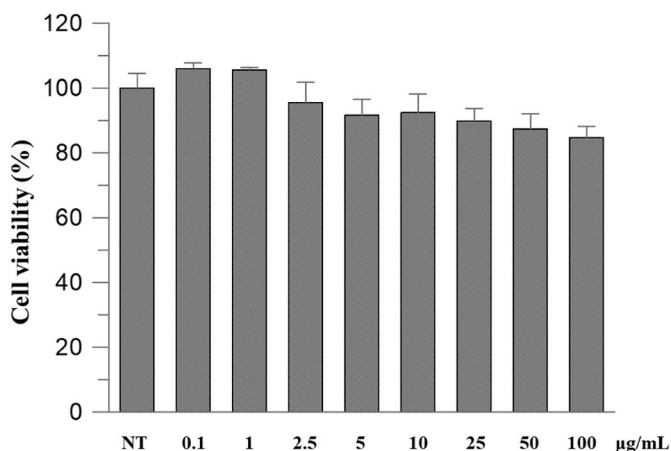


Fig. 4. Effect of FEE on Caco-2 cell viability. After 24 h of incubation with samples at different concentrations (0.1–100 µg/mL), cell viability was determined by the MTT assay. No statistically differences between treated and non-treated (NT) cells were observed.

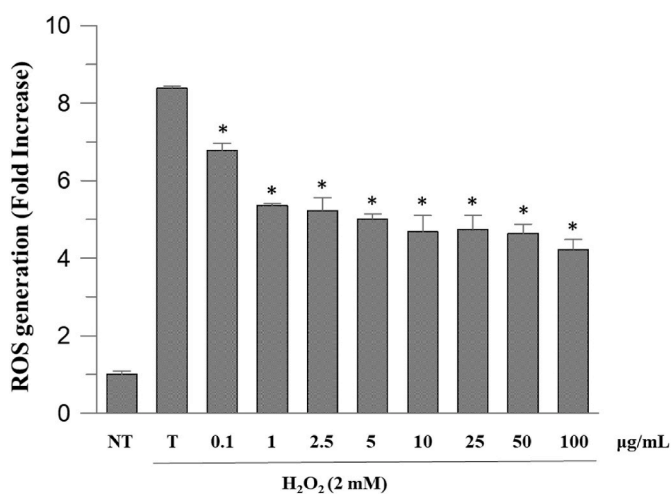


Fig. 5. Inhibition of H₂O₂-induced ROS generation (1 h-incubation with 2 mM H₂O₂) by FEE at different concentrations in Caco-2 cells. NT, non-treated cells; T, cells treated with H₂O₂ only. * Values statistically different ($p < 0.001$) from cells treated with H₂O₂.

were **lut-5og** (32), **lut-6cg** (46), **lut-7og** (51), and **5-oca** (51). All results are shown in [Table S3](#). Concerning the energies calculated with MMGBSA, the best results after the ranking were obtained by **lut-5ag** (26), **lut-5og** (39), **lut-7og** (43), and **lut-6cg** (43), which had a better rank than the control set where the best compound was topiroxostat (45) ([Table S4](#)). AutoDock ranking, on the other hand, showed that the most favorable to binding were **lut-7og** (16), **lut-5ag** (21), **3-oca** (26), **5-oca** (38), **3met-lut** (42), **lut-5og** (54), and **lut** (62), followed by febuxostat (65) ([Table S5](#)). To identify the compounds that gave favorable results in several protocols, a general ranking was made ([Table 2](#) and [Table S6](#)). The best three ligands are **lut-5ag** (100), **lut-7og** (110), and **lut-5og** (125).

Interestingly, despite generating docking grids for both Glide-XP and AutoDock with the centroid placed at the molybdenum binding site, the ligand poses obtained from the AutoDock experiments appear to be in different portions of the binding site compared to those found by Glide-XP ([Fig. S3](#)).

[Table S7](#) and [Fig. S2](#) presents the energy values for HOMO, LUMO and the energy gap results. HOMOs are primarily localized on the A-ring, whereas LUMOs are predominantly distributed between rings C

Table 2
Compounds' final ranking.

Compound	XP-Gscore	MMGBSA	BE	Final rank
lut-5ag	53	26	21	100
lut-7og	51	43	16	110
lut-5og	32	39	54	125
5-oca	51	75	38	164
3-oca	71	85	26	182
lut-7ag	56	49	97	202
lut	65	79	62	206
topiroxostat	94	45	68	207
febuxostat	55	92	65	212
lut-6cg	46	43	125	214
6met-lut	56	59	100	215
3met-lut	97	86	42	225
naringenin	74	86	70	230
8met-lut	86	97	102	285
apigenin	87	125	91	303
tisopurine	125	101	139	365
oxypurinol	133	107	130	370
allopurinol	136	131	122	389

and B. This suggests that the hydroxyl groups in the A-ring of luteolin and its derivatives are more susceptible to be attacked by free radicals ([Fig. S2](#)). The value of the HOMO-LUMO gap in a compound indicates its stability; compounds with lower energy gaps tend to be more reactive. Among the investigated ligands, **5-oca** exhibits the smallest gap (3.919 eV), followed by **3-oca** (3.965 eV), and **8met-lut** (3.970 eV) while naringenin presents the highest gap (4.541 eV).

3.3.2. Molecular dynamics

MD simulations were conducted to investigate the stability and affinity of the three best compounds (**lut-5ag**, **lut-5og**, **lut-7og**) identified through docking studies and febuxostat used as a reference compound. For each compound, MD were performed starting from the best docking poses of both AutoDock and Glide-XP software.

On average, MD simulations of AutoDock outcomes reveal lower RMSD mean values for both XO and the ligand when contrasted with those from Glide-XP results ([Table 3](#), [Fig. 6](#) and [S4](#)). The results of the MD simulations of **lut-5ag** (starting from the pose docking of Glide-XP) are not included in the graphs since the compound, exiting the binding site due to its no-stability and affinity of binding, exhibits very high RMSD values, compromising the clarity of the visualization of other data. The RMSD graph of **lut-5ag** (Glide-XP) alone is shown in [Fig. S5](#).

The trend of better results for AutoDock observed in RMSD is also confirmed in MMGBSA. The MMGBSA calculations on the trajectories indeed show superior performance in those from AutoDock compared to those derived from Glide-XP, due to the increased stability of the bonds identified. The best MMGBSA value is observed for **lut-7og** (AutoDock) with -84.5 ± 8.6 kcal/mol, which also presents the best value for Glide-XP (-43.6 ± 7.9 kcal/mol), while the worst belongs to **lut-5ag** (Glide-XP) with -11.8 ± 17.3 kcal/mol ([Table 3](#)). Considering the MD results obtained from the AutoDock poses, the RMSD values of XO throughout the entire simulation are comparable, with **lut-5og** showing slightly lower values ([Fig. 6A](#)). Lower ligand RMSD values (fit to XO) are exhibited by **lut-7og** ([Fig. 6B](#)), while febuxostat reaches excellent stability after approximately 13 ns of simulation, as confirmed by the ligand-fit RMSD as well ([Fig. 6C](#)).

The results of the trajectory clusterization are reported in [Table S8](#), which shows the population and the MMGBSA of each cluster. Comparing them with the reference frame, those derived from AutoDock trajectories exhibit a conformation more similar to the starting one ([Fig. S6](#)), while clusters from Glide-XP simulations shift slightly ([Fig. S7](#)). However, this principle cannot be applied to the clusters obtained from the **lut-5ag** trajectory (Glide-XP), as the ligand moves drastically from the starting position. During MD simulations, the compounds establish diverse interactions within the XO binding site, with varying degrees of stability. The prevalent interactions identified in

Table 3

RMSD and MMGBSA resulting from the analysis of the trajectories of MD studies. The results are presented as the mean value \pm standard deviation.

Compound	RMSD (Å)		MMGBSA (kcal/mol)	
	AutoDock	Glide-XP	AutoDock	Glide-XP
lut-7og	XO: 2.1 ± 0.2	XO: 2.0 ± 0.2	-84.5 ± 8.6	-43.6 ± 7.9
	Ligand (fit on protein): 1.4 ± 0.2	Ligand (fit on protein): 9.9 ± 1.94		
lut-5ag	Ligand (fit on ligand): 0.6 ± 0.2	Ligand (fit on ligand): 2.1 ± 0.5		
	XO: 2.1 ± 0.2	XO: 5.2 ± 8.3	-79.6 ± 10.1	-11.8 ± 17.3
lut-5og	Ligand (fit on protein): 2.3 ± 0.6	Ligand (fit on protein): 80.7 ± 19.6		
	Ligand (fit on ligand): 0.8 ± 0.14	Ligand (fit on ligand): 1.7 ± 0.3		
lut-5og	XO (fit on protein): 1.8 ± 0.1	XO (fit on protein): 2.2 ± 0.2	-69.5 ± 9.1	-42.9 ± 4.8
	Ligand (fit on protein): 2.1 ± 0.6	Ligand (fit on protein): 4.1 ± 0.6		
Febuxostat	Ligand (fit on ligand): 0.7 ± 0.5	Ligand (fit on ligand): 1.9 ± 0.2		
	XO (fit on protein): 2.1 ± 0.2	XO (fit on protein): 2.0 ± 0.2	-56.9 ± 4.9	-38.1 ± 10.3
Febuxostat	Ligand (fit on protein): 2.6 ± 0.3	Ligand (fit on protein): 5.6 ± 4.4		
	Ligand (fit on ligand): 1.7 ± 0.2	Ligand (fit on ligand): 1.5 ± 0.4		

the MD studies conducted on AutoDock outcomes are presented in [Table S9](#) and [Fig. 7](#), and the corresponding interactions from the MD simulations of Glide-XP results are displayed in [Table S10](#) and [Fig. S8](#). Overall, the poses predicted by AutoDock establish a bigger number of stable interactions than those predicted by Glide-XP. **lut-7og** establishes different H-bonds, the most significant with Ser 1082 (95 %), Met 1038 (92 %), Phe 798 (93 %), Arg 912 (85 and 73 %), and Thr 1083 (69 %) ([Fig. 7](#)) also confirmed by the calculation of interaction energies (electrostatic and van der Waals, vdW) ([Table S11](#)). In addition, the calculation of interactions finds strong vdW interactions between Gln 1040 and **lut-7og**. **lut-5ag** establishes strong electrostatic interactions with Arg 912, Asp 1084, Glu 802 and 1261, Lys 1045 and Ser 1082, and vdW interactions with Arg 912 and Gln 1042. The relevant electrostatic interactions for **lut-5og** and febuxostat are respectively with Arg 912, Ser 1082, Asp 1191, Glu 1261, and Lys 1045 ([Table S11](#)).

3.3.3. In silico ADME predictions

[Table 4](#) displays the results obtained from QikProp. All three compounds are predicted to be inactive towards the CNS and are not expected to be permeable in Caco-2 and MDCK models. The forecasted human oral absorption does not seem optimal, as unfavorable results are observed both qualitatively and quantitatively. There are no significant breaches of Lipinski's rule of five, considering molecular weight, rotatable bonds, H-bond donor and acceptor groups. For a comprehensive list of predicted ADME properties from QikProp, refer to [Table S12](#).

3.4. Luteolin 7-O-glucoside XO inhibitory activity

Considering that luteolin 7-O-glucoside achieved the highest molecular dynamics score and stability, we tested it *in vitro* against XO. The compound showed good inhibitory activity with an IC₅₀ value of 4.8 ± 0.42 $\mu\text{g/mL}$, equivalent to 12.6 ± 1.1 μM , 2.3-fold better than the standard inhibitor allopurinol (IC₅₀ 11.5 ± 0.8 $\mu\text{g/mL}$, equivalent to 43.5 ± 3.0 μM).

In comparison, febuxostat, exhibited an IC₅₀ value of 0.05 ± 0.002 $\mu\text{g/mL}$, equivalent to 0.13 ± 0.04 μM , significantly surpassing both **lut-7og** and allopurinol in inhibitory potency. This aligns with existing literature acknowledging febuxostat's superior efficacy as an XO inhibitor. However, it is primarily prescribed as a second-line treatment due to potential adverse effects.

The mode of inhibition was also determined by varying the concentration of substrate and inhibitor. This kinetic analysis indicates that it acts as a mixed-type inhibitor ([Fig. 8A](#)). The values of K_i and K_{iS} constants for binding of the compound to the free enzyme or the enzyme-substrate complex were also calculated from the secondary plots ([Fig. 8B](#) and [C](#), respectively). The K_i value was 1.06 $\mu\text{g/mL}$, while the K_{iS} was equal to 3.51 $\mu\text{g/mL}$.

Additionally, compounds 3oca and 5oca, which ranked among the top six in the docking final ranking, were also tested but showed IC₅₀ values greater than 50 μM .

4. Discussion

The investigation into *A. microcarpus* extracts for XO inhibitory activity revealed that the FEE exhibited remarkable inhibition of XO. Additionally, consistent with these and prior studies, the FEE demonstrated antioxidant capabilities. Among the previously identified phenolic compounds in FEE [[13](#)], luteolin, already known for its inhibitory effects on XO and its antioxidant activity, and other derivatives were identified.

We conducted initial different molecular docking studies followed by subsequent molecular dynamics simulations to discern the XO inhibitory potential within the previously identified compounds. Thirteen compounds from the FEE underwent analysis, employing a consensus docking protocol with two different software tools (Glide-XP with subsequent MMGBSA calculation and AutoDock) and integrating data from eight distinct X-rays of XO. The consensus-score docking protocol was applied to strengthen the results and select the top 3 compounds (**lut-7og**, **lut-5og**, and **lut-5ag**) for further molecular dynamics studies. To ensure data robustness, the dynamics of the top 3 compounds were simulated using the best poses from both software platforms. Molecular dynamics studies revealed the superior binding achieved by AutoDock for all three compounds. Specifically, **lut-7og** exhibited exceptional binding stability by exhibiting the lowest RMSD values and the most favorable MMGBSA energies throughout the 250 ns simulation on both software platforms, indicating excellent binding energy and stability of **lut-7og**. Consequently, we tested the ability of **lut-7og** to inhibit XO *in vitro*, and we found that it is more effective than the standard inhibitor allopurinol. Although **lut-7og** showed potent *in vitro* inhibitory activity against XO, surpassing allopurinol, it did not demonstrate greater potency than febuxostat, which is acknowledged in the literature as the most potent XO inhibitor, but it is considered a second-line treatment option due to its side effects. The initial docking studies positioned **lut-7og** as a potentially superior inhibitor to febuxostat. The dynamics studies starting from the pose obtained from AutoDock have highlighted that febuxostat achieves excellent binding stability after 13 ns of simulation. However, the *in vitro* results did not align with docking predictions. This discrepancy is not entirely unexpected. Molecular docking, while a valuable screening tool, does not fully account for factors such as solubility and stability, which are pivotal in determining a compound's inhibitory efficiency in a biological context.

These findings contribute to understanding *A. microcarpus* as a potential source of xanthine oxidase inhibitors, with implications for natural medicine and oxidative stress-related conditions.

It is important to note that *in silico* ADME studies have revealed that **lut-7og** currently lacks satisfactory pharmacokinetic characteristics, particularly demonstrating poor cellular permeability. To unlock its potential for drug utilization, optimization studies are imperative. Key pharmacological techniques, such as prodrug development, formulation enhancements, and the utilization of nanotechnology [[44](#)], should be

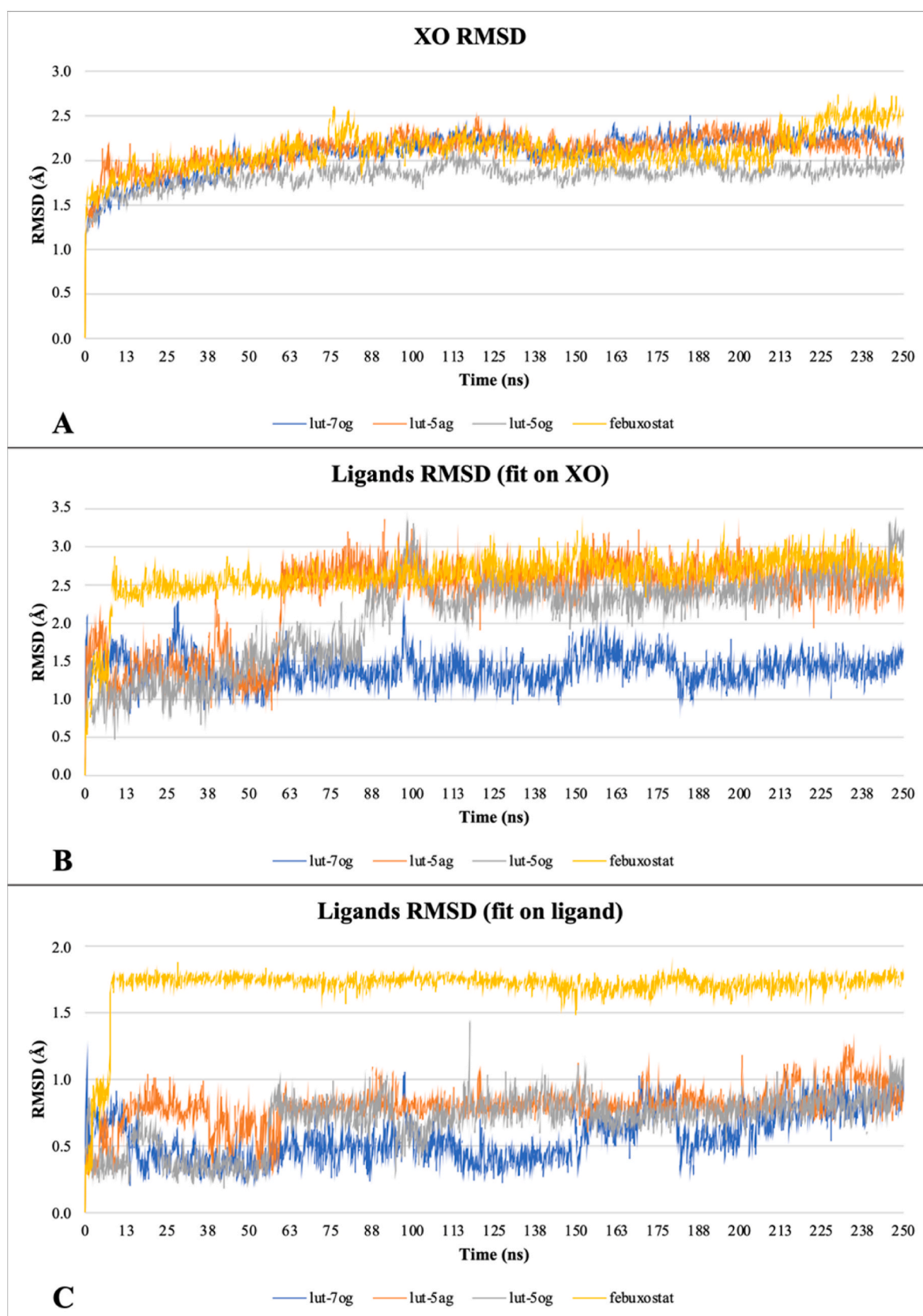


Fig. 6. Graph of RMSD during the conducted MD simulations starting from the best poses obtained with AutoDock. The x-axis shows the frame number simulation time in ns, while the y-axis represents the RMSD in Å. Lut-7og is represented in blue, lut-5og in grey and febuxostat in yellow. **A:** Representation of XO RMSD during 250 ns. **B:** Representation of ligands RMSD fit on XO during 250 ns. **C:** Representation of ligands RMSD fit on ligand during 250 ns.

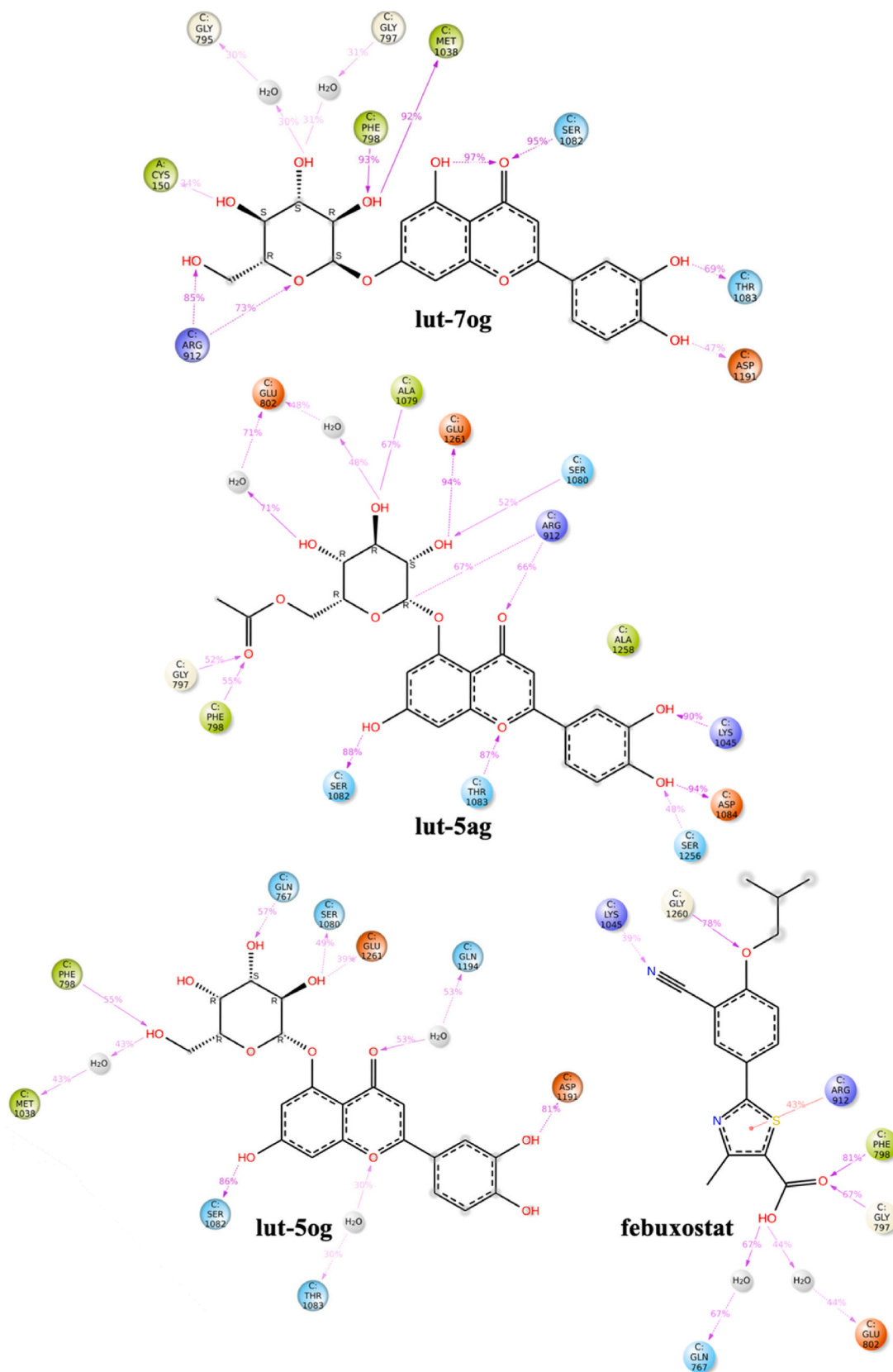


Fig. 7. 2D representation of most frequent interactions (present for more than 30% of the simulation time) identified by MD experiments of the top compounds based on AutoDock poses. Purple arrows represent H-bonds and water bridges, while red lines represent π -cation interactions. In each interaction, the percentage of interaction during the 250 ns of molecular dynamics is displayed. The color intensity of the arrows is determined by the percentage of interaction, with higher presence resulting in a more intense color.

Table 4
In silico ADME prediction of lut-7ag, lut-7og and lut-5ag.

	Recommended range	lut-7og	lut-5og	lut-5ag
LogP				
Number of violations of Lipinski's rule of five	<4	2	2	2
Number of violations of Jorgensen's rule of three	<3	2	2	1
MDCK cell permeability in nm/sec	<25 poor; >500 great	1	1	1
Number of likely metabolic reactions	1–8			
Predicted apparent Caco-2 cell permeability in nm/sec	<25 poor; >500 great	3	4	4
Predicted of human oral absorption	<25 % poor; >80 % high	poor	poor	Poor
CNS activity	–2 inactive; 2 active	–2	–2	–2
Predicted HERG activity	concern below 5			

explored to address and improve the observed limitations in cellular permeability.

5. Conclusion

Our research on extracts of *Asphodelus microcarpus* has shown that the ethanol extract of its flowers has strong antioxidant properties and inhibits xanthine oxidase. Molecular docking and dynamics simulations revealed that luteolin 7-O-glucoside, a compound previously identified in this extract, has a particularly stable and potent inhibitory effect on xanthine oxidase. For its *in vivo* application, studies will be required to enhance its pharmacokinetics without compromising its inhibitory effect on XO.

Financial interests

One of the authors have any financial interests or arrangements with any organizations that could potentially gain or lose financially from the publication of this work.

Personal relationships

No author has any personal relationships with individuals or organizations that could influence or bias the research, interpretation, or presentation of the findings.

Professional affiliations

The research was conducted with the aim of advancing scientific knowledge and without any external influence from affiliated institutions.

Funding

The research received no external funding, and the authors did not receive financial support from any external sources for this work.

Other interests

The authors declare no other interests that might be perceived as having influenced the research.

CRedit authorship contribution statement

Amalia Di Petrillo: Writing – original draft, Supervision, Methodology, Investigation, Formal analysis, Conceptualization. **Chiara Siguri:**

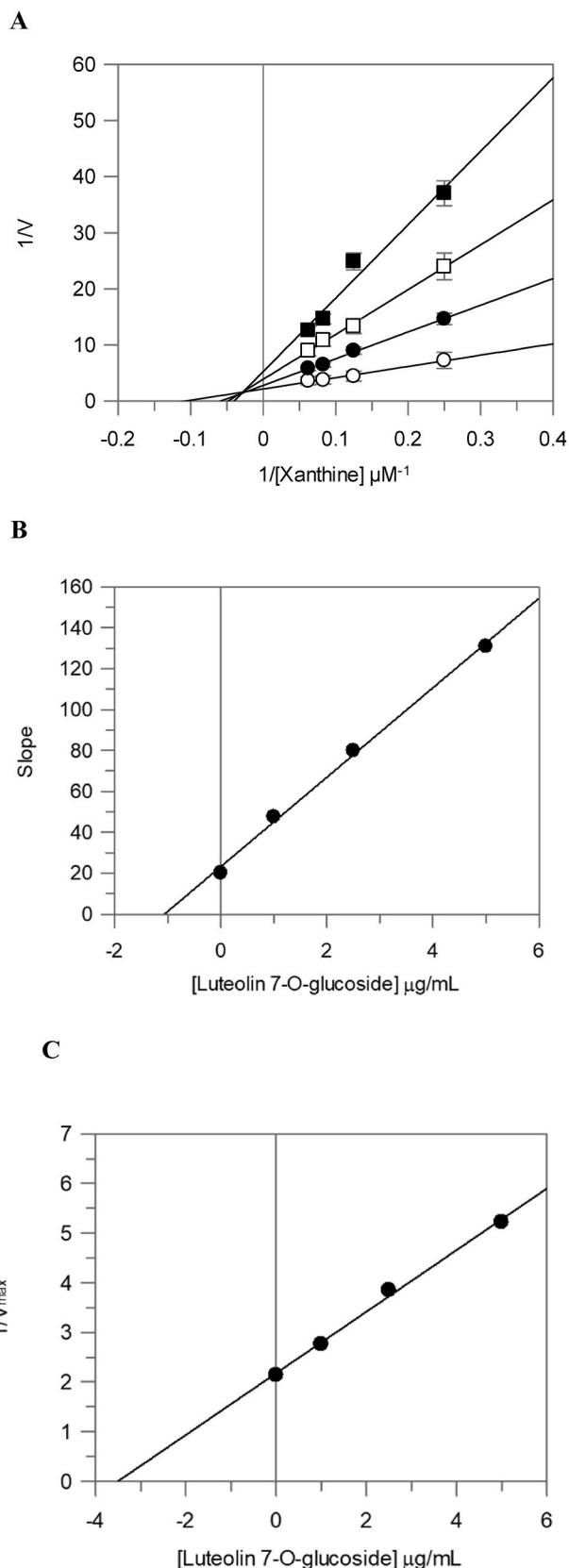


Fig. 8. Inhibition of XO activity by luteolin 7-O-glucoside. A: Lineweaver-Burk plot for inhibition of luteolin 7-O-glucoside on XO activity using xanthine as substrate. Inhibitor concentrations were: 0 (○), 1 µg/mL (●), 2.5 µg/mL (□) and 5 µg/mL (■). B: Replot of the slope values versus compound concentration. C: Replot of the $1/V_{max}$ values versus compound concentration.

Writing – original draft, Software, Methodology, Investigation, Formal analysis, Data curation. **Giovanna L. Delogu**: Writing – review & editing, Investigation. **Antonella Fais**: Writing – review & editing, Methodology, Investigation, Formal analysis. **Benedetta Era**: Writing – review & editing. **Sonia Floris**: Writing – review & editing, Methodology, Investigation, Formal analysis, Data curation. **Francesca Pintus**: Writing – review & editing, Methodology, Investigation. **Amit Kumar**: Writing – review & editing. **Massimo Claudio Fantini**: Writing – review & editing. **Stefania Olla**: Writing – original draft, Supervision, Methodology, Investigation, Funding acquisition, Formal analysis.

Declaration of competing interest

The authors of this manuscript, entitled “Exploring *Asphodelus microcarpus* as a Source of Xanthine Oxidase Inhibitors: Insights from In Silico and In Vitro Studies,” declare the following interests.

Data availability

No data was used for the research described in the article.

Appendix A. Supplementary data

Supplementary data to this article can be found online at <https://doi.org/10.1016/j.cbi.2024.111087>.

References

- C.J. Chen, J.M. Lü, Q. Yao, Hyperuricemia-related diseases and xanthine oxidoreductase (XOR) inhibitors: an overview, *Med. Sci. Mon. Int. Med. J. Exp. Clin. Res.* 22 (2016) 2501–2512, <https://doi.org/10.12659/MSM.899852>.
- G. Schwarz, R.R. Mendel, M.W. Ribbe, Molybdenum cofactors, enzymes and pathways, *Nature* (2009) 839–847, <https://doi.org/10.1038/nature08302>, 2009 460:7257 460.
- A. Kushiyama, Y. Nakatsu, Y. Matsunaga, T. Yamamotoya, K. Mori, K. Ueda, Y. Inoue, H. Sakoda, M. Fujishiro, H. Ono, T. Asano, Role of uric acid metabolism-related inflammation in the pathogenesis of metabolic syndrome components such as atherosclerosis and nonalcoholic steatohepatitis, *Mediat. Inflamm.* 2016 (2016), <https://doi.org/10.1155/2016/8603164>.
- T.T. Braga, M.F. Forni, M. Correa-Costa, R.N. Ramos, J.A. Barbutto, P. Branco, A. Castoldi, M.I. Hiyane, M.R. Davanzo, E. Latz, B.S. Franklin, A.J. Kowaltowski, N. O.S. Camara, Soluble uric acid activates the NLRP3 inflammasome, *Sci. Rep.* 7 (1 7) (2017) 1–14, <https://doi.org/10.1038/srep39884>, 2017.
- M.A. Martillo, L. Nazzari, D.B. Crittenden, The crystallization of monosodium urate, *Curr. Rheumatol. Rep.* 16 (2014) 1–8, <https://doi.org/10.1007/S11926-013-0400-9/METRICS>.
- P. Pacher, A. Nivorozhkin, C. Szabó, Therapeutic effects of xanthine oxidase inhibitors: renaissance half a century after the discovery of allopurinol, *Pharmacol. Rev.* 58 (2006) 87–114, <https://doi.org/10.1124/PR.58.1.6>.
- R.S. Almeer, S.F. Hammad, O.F. Leheta, A.E. Abdel Moneim, H.K. Amin, Anti-inflammatory and anti-hyperuricemic functions of two synthetic hybrid drugs with dual biological active sites, *Int. J. Mol. Sci.* 20 (2019) E5635, <https://doi.org/10.3390/IJMS20225635>, E5635.
- D. Tungmunthum, A. Thongboonyou, A. Pholboon, A. Yangsabai, Flavonoids and other phenolic compounds from medicinal plants for pharmaceutical and medical aspects: an overview, *Medicines (Basel)* 5 (2018) 93, <https://doi.org/10.3390/MEDICINES5030093>.
- V. Mohos, E. Fliszár-Nyúl, M. Poór, Inhibition of xanthine oxidase-catalyzed xanthine and 6-mercaptopurine oxidation by flavonoid aglycones and some of their conjugates, *Int. J. Mol. Sci.* 21 (2020), <https://doi.org/10.3390/IJMS21093256>.
- M.R. de Souza, C.A. de Paula, M.L. Pereira de Resende, A. Grabe-Guimarães, J. D. de Souza Filho, D.A. Saúde-Guimarães, Pharmacological basis for use of *Lychonophora trichocarpha* in gouty arthritis: anti-hyperuricemic and anti-inflammatory effects of its extract, fraction and constituents, *J. Ethnopharmacol.* 142 (2012) 845–850, <https://doi.org/10.1016/j.jep.2012.06.012>.
- N. Mayouf, N. Charef, S. Saoudi, A. Baghiani, S. Khenouf, L. Arrar, Antioxidant and anti-inflammatory effect of *Asphodelus microcarpus* methanolic extracts, *J. Ethnopharmacol.* 239 (2019), <https://doi.org/10.1016/J.JEP.2019.111914>.
- A. Di Petrillo, A. Fais, F. Pintus, C. Santos-Buelga, A.M. González-Paramás, V. Piras, G. Orrù, A. Mameli, E. Tramontano, A. Frau, Broad-range potential of *Asphodelus microcarpus* leaves extract for drug development, *BMC Microbiol.* 17 (2017) 1–9, <https://doi.org/10.1186/S12866-017-1068-5/TABLES/3>.
- A. Di Petrillo, A.M. González-Paramás, B. Era, R. Medda, F. Pintus, C. Santos-Buelga, A. Fais, Tyrosinase inhibition and antioxidant properties of *Asphodelus microcarpus* extracts, *BMC Compl. Alternative Med.* 16 (2016), <https://doi.org/10.1186/S12906-016-1442-0>.
- J. Yan, G. Zhang, Y. Hu, Y. Ma, Effect of luteolin on xanthine oxidase: inhibition kinetics and interaction mechanism merging with docking simulation, *Food Chem.* 141 (2013) 3766–3773, <https://doi.org/10.1016/J.FOODCHEM.2013.06.092>.
- A. Di Petrillo, C. Santos-Buelga, B. Era, A.M. González-Paramás, C.I.G. Tuberoso, R. Medda, F. Pintus, A. Fais, Sardinian honeys as sources of xanthine oxidase and tyrosinase inhibitors, *Food Sci. Biotechnol.* 27 (2018) 139, <https://doi.org/10.1007/S10068-017-0275-Z>.
- P. Kumar, A. Nagarajan, P.D. Uchil, Analysis of cell viability by the MTT assay, *Cold Spring Harb. Protoc.* (2018) 469–471, <https://doi.org/10.1101/PDB.PROT095505>, 2018.
- H. Kim, X. Xue, Detection of total reactive oxygen species in adherent cells by 2',7'-dichlorodihydrofluorescein diacetate staining, *J. Vis. Exp.* 2020 (2020) 1–5, <https://doi.org/10.3791/60682>.
- H.M. Berman, J. Westbrook, Z. Feng, G. Gilliland, T.N. Bhat, H. Weissig, I. N. Shindyalov, P.E. Bourne, The protein Data Bank, *Nucleic Acids Res.* 28 (2000) 235–242, <https://doi.org/10.1093/NAR/28.1.235>.
- C. Enroth, B.T. Eger, K. Okamoto, T. Nishino, T. Nishino, E.F. Pai, Crystal structures of bovinemilk xanthine dehydrogenase and xanthine oxidase: structure-based mechanism of conversion, *Proc. Natl. Acad. Sci. U. S. A.* 97 (2000) 10723–10728, <https://doi.org/10.1073/PNAS.97.20.10723/ASSET/3F1B339E-2704-4CB9-A9B4-009CDCE6D6A1B/ASSETS/GRAPHIC/PQ1903518005.JPEG>.
- M. Kanbay, S. Copur, L. Ozbek, A. Mutlu, D. Cejka, P. Ciceri, M. Cozzolino, M. L. Haarhaus, Klotho: a potential therapeutic target in aging and neurodegeneration beyond chronic kidney disease—a comprehensive review from the ERA CKD-MBD working group, *Clin Kidney J* 17 (2024) 1–11, <https://doi.org/10.1093/CKJ/SFAD276>.
- E.S. Di Cairano, A.M. Davalli, L. Perego, S. Sala, V.F. Sacchi, S. La Rosa, G. Finzi, C. Placidi, C. Capella, P. Conti, V.E. Centonze, F. Casiraghi, F. Bertuzzi, F. Folli, C. Perego, The glial glutamate transporter 1 (GLT1) is expressed by pancreatic beta-cells and prevents glutamate-induced beta-cell death, *J. Biol. Chem.* 286 (2011) 14007–14018, <https://doi.org/10.1074/JBC.M110.183517>.
- H. Cao, J. Hall, R. Hille, X-ray crystal structure of arsenite-inhibited xanthine oxidase: μ -sulfido, μ -oxo double bridge between molybdenum and arsenic in the active site, *J. Am. Chem. Soc.* 133 (2011) 12414–12417, https://doi.org/10.1021/JA2050265/SUPPL_FILE/JA2050265_SI_001.PDF.
- H. Cao, J. Hall, R. Hille, Substrate orientation and specificity in xanthine oxidase: crystal structures of the enzyme in complex with indole-3-acetaldehyde and guanine, *Biochemistry* 53 (2014) 533–541, <https://doi.org/10.1021/Bi401465U>.
- H. Cao, J.M. Pauff, R. Hille, X-ray crystal structure of a xanthine oxidase complex with the flavinoid inhibitor quercetin, *J. Nat. Prod.* 77 (2014) 1693–1699, https://doi.org/10.1021/NP500320G/ASSET/IMAGES/MEDIUM/NP-2014-00320G_0006.GIF.
- Schrödinger Software Release 2022-1 | Macs in Chemistry, (n.d.). <https://www.maccinchem.org/blog/files/279f5ca3fa90d6b7db20ad4b0afed0-2841.php> (accessed May 17, 2023).
- C.R. Søndergaard, M.H.M. Olsson, M. Rostkowski, J.H. Jensen, Improved treatment of ligands and coupling effects in empirical calculation and rationalization of p K a values, *J. Chem. Theor. Comput.* 7 (2011) 2284–2295, https://doi.org/10.1021/CT200133Y/SUPPL_FILE/CT200133Y_SI_001.PDF.
- A.D. Bochevarov, E. Harder, T.F. Hughes, J.R. Greenwood, D.A. Braden, D. M. Philipp, D. Rinaldo, M.D. Halls, J. Zhang, R.A. Friesner, Jaguar: a high-performance quantum chemistry software program with strengths in life and materials sciences, *Int. J. Quant. Chem.* 113 (2013) 2110–2142, <https://doi.org/10.1002/QUA.24481>.
- C. Lu, C. Wu, D. Ghoreishi, W. Chen, L. Wang, W. Damm, G.A. Ross, M.K. Dahlgren, E. Russell, C.D. Von Barga, R. Abel, R.A. Friesner, E.D. Harder, OPLS4: improving force field accuracy on challenging regimes of chemical space, *J. Chem. Theor. Comput.* 17 (2021) 4291–4300, https://doi.org/10.1021/ACS.JCTC.1C00302/SUPPL_FILE/CT1C00302_SI_002.ZIP.
- T. Van Mourik, M. Bühl, M.P. Gaiete, Density functional theory across chemistry, physics and biology, *Phil. Trans. Math. Phys. Eng. Sci.* 372 (2014), <https://doi.org/10.1098/RSTA.2012.0488>.
- A.D. Becke, Density-functional thermochemistry. III. The role of exact exchange, *J. Chem. Phys.* 98 (1993) 5648–5652, <https://doi.org/10.1063/1.464913>.
- R.A. Friesner, J.L. Banks, R.B. Murphy, T.A. Halgren, J.J. Klicic, D.T. Mainz, M. P. Repasky, E.H. Knoll, M. Shelley, J.K. Perry, D.E. Shaw, P. Francis, P.S. Shenkin, Glide: a new approach for rapid, accurate docking and scoring. 1. Method and assessment of docking accuracy, *J. Med. Chem.* 47 (2004) 1739–1749, https://doi.org/10.1021/JM0306430/SUPPL_FILE/JM0306430_S.PDF.
- S. Genheden, U. Ryde, The MM/PBSA and MM/GBSA methods to estimate ligand-binding affinities, *Expert Opin. Drug Discov.* 10 (2015) 449–461, <https://doi.org/10.1517/17460441.2015.1032936>.
- J. Li, R. Abel, K. Zhu, Y. Cao, S. Zhao, R.A. Friesner, The VSGB 2.0 model: a next generation energy model for high resolution protein structure modeling, *Proteins: Struct., Funct., Bioinf.* 79 (2011) 2794–2812, <https://doi.org/10.1002/PROT.23106>.
- J. Gasteiger, M. Marsili, A new model for calculating atomic charges in molecules, *Tetrahedron Lett.* 19 (1978) 3181–3184, [https://doi.org/10.1016/S0040-4039\(01\)94977-9](https://doi.org/10.1016/S0040-4039(01)94977-9).
- M.A.S. Sallem, S.A. De Sousa, F.J.D.S. E Silva, AutoGrid: towards an automatic grid middleware. Proceedings of the Workshop on Enabling Technologies: Infrastructure for Collaborative Enterprises, WETICE, 2007, pp. 223–228, <https://doi.org/10.1109/WETICE.2007.4407158>.
- G.M. Morris, H. Ruth, W. Lindstrom, M.F. Sanner, R.K. Belew, D.S. Goodsell, A. J. Olson, AutoDock4 and AutoDockTools4: automated docking with selective

- receptor flexibility, *J. Comput. Chem.* 30 (2009) 2785–2791, <https://doi.org/10.1002/JCC.21256>.
- [37] N. Moitessier, P. Englebienne, D. Lee, J. Lawandi, C.R. Corbeil, Towards the development of universal, fast and highly accurate docking/scoring methods: a long way to go, *Br. J. Pharmacol.* 153 (2008) S7–S26, <https://doi.org/10.1038/SJ.BJP.0707515>.
- [38] X.-Y. Meng, H.-X. Zhang, M. Mezei, M. Cui, Molecular docking: a powerful approach for structure-based drug discovery, *Curr. Comput. Aided Drug Des.* 7 (2011) 146–157, <https://doi.org/10.2174/157340911795677602>.
- [39] K.J. Bowers, D.E. Chow, H. Xu, R.O. Dror, M.P. Eastwood, B.A. Gregersen, J. L. Klepeis, I. Kolossvary, M.A. Moraes, F.D. Sacerdoti, J.K. Salmon, Y. Shan, D. E. Shaw, Scalable algorithms for molecular dynamics simulations on commodity clusters, 43–43, <https://doi.org/10.1109/SC.2006.54>, 2007.
- [40] W.L. Jorgensen, J. Chandrasekhar, J.D. Madura, R.W. Impey, M.L. Klein, Comparison of simple potential functions for simulating liquid water, *J. Chem. Phys.* 79 (1983) 926–935, <https://doi.org/10.1063/1.445869>.
- [41] W.G. Hoover, Canonical dynamics: equilibrium phase-space distributions, *Phys. Rev.* 31 (1985) 1695, <https://doi.org/10.1103/PhysRevA.31.1695>.
- [42] G.J. Martyna, D.J. Tobias, M.L. Klein, Constant pressure molecular dynamics algorithms, *J. Chem. Phys.* 101 (1994) 4177–4189, <https://doi.org/10.1063/1.467468>.
- [43] B.J. Frey, D. Dueck, Clustering by passing messages between data points, *Science* 315 (2007) 972–976, https://doi.org/10.1126/SCIENCE.1136800/SUPPL_FILE/FREY.SOM.PDF, 1979.
- [44] J. Rautio, N.A. Meanwell, L. Di, M.J. Hageman, The expanding role of prodrugs in contemporary drug design and development, *Nat. Rev. Drug Discov.* 17 (2018) 559–587, <https://doi.org/10.1038/NRD.2018.46>.